

# Eolian cannibalism: Reworked loess and fluvial sediment as the main sources of the Chinese Loess Plateau

A. Licht<sup>1,2,3,†</sup>, A. Pullen<sup>1,4</sup>, P. Kapp<sup>1</sup>, J. Abell<sup>1</sup>, and N. Giesler<sup>1</sup>

<sup>1</sup>Department of Geosciences, University of Arizona, Tucson, Arizona 85721, USA

<sup>2</sup>Biodiversity Institute, University of Kansas, Lawrence, Kansas 66045, USA

<sup>3</sup>Institut für Erd- und Umweltwissenschaften, Potsdam Universität, 14476 Potsdam, Germany

<sup>4</sup>Department of Earth and Environmental Sciences, University of Rochester, Rochester, New York 14627, USA

## ABSTRACT

The loess and paleosol sequences of the Chinese Loess Plateau are composed of Quaternary dust, the origin of which has been the subject of considerable debate. Some recent U-Pb geochronological studies of eolian zircons have proposed the existence of two major wind pathways: from the north and northwest, through the Badan Jaran, Tengger, and Mu Us Deserts during interglacials, and from the west, through the Qaidam Basin during glacials. Others have emphasized the importance of Yellow River sediment supply in the Chinese Loess Plateau sediment budget. However, tracking dust source regions through U-Pb dating in a statistically robust manner is particularly complex given the similar age peaks in the age probability distributions of potential source regions in Central Asia. This paper presents 2410 new U-Pb ages of detrital zircons from wind-eroded strata, Quaternary eolian deposits, and modern river sands in central China in order to increase the robustness and the spatial resolution of zircon age distributions in dust source regions. We then propose a new mixture modeling technique to statistically address the contribution of these different sources to the Chinese Loess Plateau sedimentary budget. Our contribution estimates indicate that eolian supply to the Chinese Loess Plateau is dominated (60%–70%) by reworking of Yellow River sediment. Moreover, evidence of Qaidam Basin-sourced zircons (15%–20%) in both loess (glacial) and paleosol (interglacial) layers corroborates the existence of an erosive wind pathway through the Qaidam Basin during glacials and implies that a substantial portion of the interglacial dust is recycled from older glacial loess. We

**propose that sediment reworking of Yellow River sediment and older loess deposits by wind on the Chinese Loess Plateau homogenized the eolian zircon populations toward a glacial provenance due to higher (2–20 times) dust accumulation rates during glacials. These findings suggest that the Chinese Loess Plateau has evolved as a more dynamic landform than previous thought, where wind deflation, fluvial input, lateral transport, and accumulation of sediment are equally important. These internal reworking effects would then significantly bias the paleoclimatic interpretations based on eolian dust properties of the Chinese Loess Plateau.**

## INTRODUCTION

The Chinese Loess Plateau (Fig. 1) is mainly composed of eolian dust deposits that are predominantly brought by spring storms sweeping clastic material from the deserts of the Asian interior (Roe, 2009). Though the oldest loess deposits within the southernmost and westernmost Chinese Loess Plateau have been dated to 8 Ma (An et al., 2001), 22–25 Ma (Guo et al., 2002; Qiang et al., 2011), and 41 Ma (Licht et al., 2014), most of the Chinese Loess Plateau is composed of Quaternary loess-paleosol sequences. Loess layers were deposited during glacial periods under a colder and drier Asian climate, whereas paleosol layers developed during warmer and moister interglacial periods with enhanced summer monsoons (An et al., 1990; Porter and An, 1995; Kang et al., 2011, 2013).

Loess deposits consist of a coarse (12–70  $\mu\text{m}$ ) primary fraction, transported via saltation by dust storms in near-surface suspension clouds, and a fine (1–3  $\mu\text{m}$ ) secondary fraction, the origin of which is still controversial, either pedogenic, supplied by upper-level airflow, and/or by adherence to the coarse fraction (Derbyshire et al., 1998; Sun et al., 2006; Stevens and Lu,

2009; Vandenberghe, 2013). In the modern interglacial climate, dust storms originate north and northwest of the Chinese Loess Plateau, in the Gobi Desert, commonly during the breakdown of the Siberian High in Spring (Roe, 2009), and they track across the Badan Jaran, Tengger, and Mu Us Deserts (Wang et al., 2004). These desert areas are thought to be the main source areas for the coarse fraction of the modern dust to the plateau, though the exact locus of dust generation in these regions—piedmont alluvial fans, dried lake basins, or sand dune fields—is widely debated (Pye, 1995; Sun, 2002; Amit et al., 2014). Additionally, recent provenance studies of loess have also highlighted the importance of reworking of local substratum rocks (mostly pre-Quaternary terrestrial sediment) and of fluvial detritus brought by the Yellow River, with headwaters in northeastern Tibet (Fig. 1), in the loess sedimentary budget (Stevens et al., 2013; Che and Li, 2013; Bird et al., 2015; Nie et al., 2015; Kapp et al., 2015).

The geographic origin of pre-Holocene glacial loess is more controversial. Wind-eroded landforms in the Qaidam Basin (Kapp et al., 2011; Rohrmann et al., 2013), U-Pb geochronology of eolian zircons (Pullen et al., 2011), and grain-size data and climate simulations (Vandenberghe et al., 2006) have suggested the existence of a different dust-storm track during glacial periods. These observations point to the loci of source areas located south of the Qilian Shan mountain ranges, in the Qaidam Basin and northern Tibetan Plateau (Fig. 1). This arid region would have been deflated by surface westerly winds, in response to either enhanced penetration of Atlantic westerlies during glacial periods (Vandenberghe et al., 2006), and/or to the shift of the whole midlatitude atmospheric system by  $\sim 10^\circ$  of latitude equatorward (Toggweiler and Russell, 2008; Kapp et al., 2011). In deeper time, this westerly wind pathway would have been favored by a lower-elevation north-

<sup>†</sup>licht@uw.edu

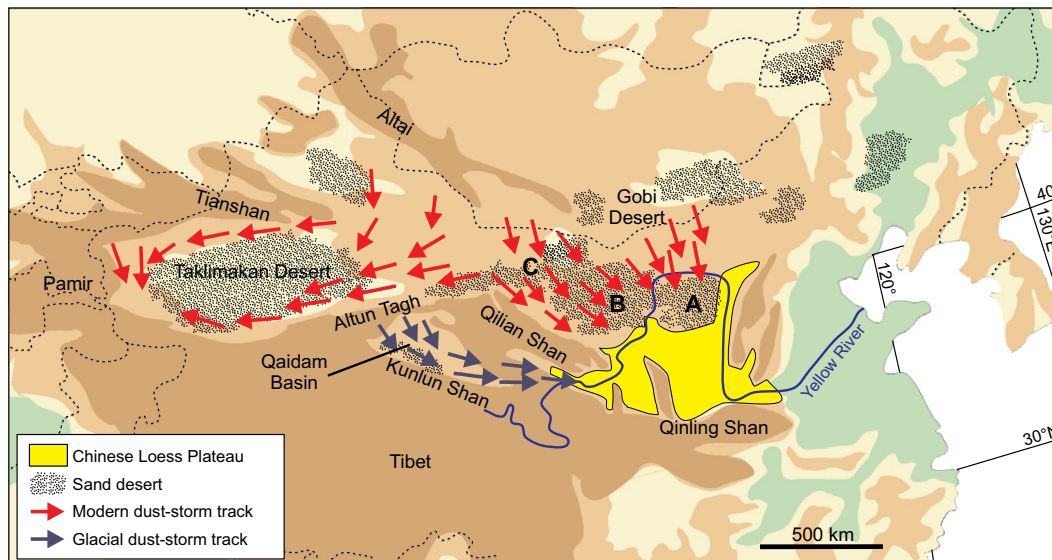


**Figure 1.** Schematic map of Central Asia, showing the modern, simplified dust-storm tracks and near-surface wind patterns (red arrows), throughout the (A) Mu Us, (B) Tengger, and (C) Badan Jaran Deserts, and the hypothetical “glacial” dust-storm track (blue arrows), through the Qaidam Basin and across northern and central Tibet (Pullen et al., 2011).

ern Tibetan Plateau until the late Neogene–early Quaternary (Sun et al., 2008; Nie et al., 2014). However, the relative contributions from the Qaidam Basin compared with that of the more proximal desert regions and the Yellow River to the north in the eolian sedimentary budget are poorly constrained, given the complexity of the provenance problem with multiple potential source regions.

Single-grain U-Pb dating of detrital zircons is an efficient and effective technique to differentiate the contribution of discrete sources in sediment samples (Gehrels, 2000). U-Pb analyses of detrital zircon grains produce age distributions that reflect the ages of zircons in the source rocks for the sediment. The presence or absence of a particular age group in a sample is used as a test to determine if a particular source region contributes to the sample (Gehrels et al., 2011). Recent developments in laser-ablation techniques allow for U-Pb analyses of small (<40  $\mu\text{m}$ ) zircons in eolian dust and application of this method to Chinese loess deposits (Stevens et al., 2010, 2013; Pullen et al., 2011; Xiao et al., 2012; Che and Li, 2013; Nie et al., 2014; Bird et al., 2015). Tracking Chinese loess dust source regions through U-Pb dating is particularly complex given the similar age peaks in the age probability distributions of western and northern deserts in central China, as well as in individual mountain ranges and terranes (Gehrels et al., 2003, 2011; Stevens et al., 2010). Central Asian age distributions of detrital and igneous rocks are commonly dominated by two major age groups, 225–330 Ma and 380–500 Ma, with two secondary, broader age populations, 750–1000 Ma and 1500–2800 Ma, the relative contribution of which varies regionally (Gehrels et al., 2003; Stevens et al., 2010; Pullen

et al., 2011; Lease et al., 2007, 2012; Weislogel et al., 2010). However, the number ( $n$ ) of U-Pb ages per published loess sample (commonly  $n < 150$ ) is so far too low to accurately constrain the relative contribution of each age group (see next section; e.g., Andersen, 2005; Pullen et al., 2014). Some workers have been using the multi-dimensional scaling (MDS) statistical technique of Vermeesch (2013), based on the less  $n$ -dependent Kolmogorov-Smirnov (KS) statistic, as a visualization tool to qualitatively estimate the similarity (or dissimilarity) between loess samples and potential sources (Stevens et al., 2013; Che and Li, 2013; Bird et al., 2015). However, this approach does not provide quantitative estimates of the relative contribution of the different dust source regions.

This paper presents new U-Pb ages of detrital zircons from eolian and fluvial deposits as well as from wind-eroded strata in central China, in order to better illuminate the zircon age distributions in potential dust source regions. We then present a new mixture modeling technique that statistically determines the contribution of different sources based on U-Pb data, and we use it to assess the provenance of the Chinese Loess Plateau.

## SAMPLES AND METHODS

### Sampling Strategy

We first expanded the data set of existing U-Pb ages surrounding the Chinese Loess Plateau with 23 new samples to capture regional variability in eolian sediment source. Surface samples of up to 4 kg were collected from various locations in central China (Fig. 2). In the arid areas north and west of the Chinese Loess

Plateau, we sampled modern eolian sand dunes (one sample in the Mu Us Desert, four in the Tengger Desert, and two in the Badan Jaran Desert). We also sampled the tops of yardangs (three samples in the Mu Us Desert and four in the Badan Jaran Desert), streamlined landforms sculpted by windblown sand and composed of Pliocene–Quaternary to Cretaceous sedimentary bedrock. In the western, deflationary, and bedrock-floored Qaidam Basin, we sampled Miocene–Pliocene strata that have been sculpted into yardangs (three samples, which were previously assessed using cosmogenic nuclides by Rohrmann et al., 2013). To represent the average influx of sediment from northeast Tibet, we sampled modern fluvial deposits from the Yellow River at the western edge of the Mu Us Desert (one sample). We also determined new U-Pb ages on zircons from paleosol layers in the Heimugou section (layers S0, S1, S9, S15 and S22; after Porter, 2001) of the central Chinese Loess Plateau.

We determined U-Pb ages on ~70 to ~370 detrital zircons per sample. In total, we increased the existing data set of Central Asian U-Pb ages by 2410 ages from 23 samples. The nature, location, and number of U-Pb ages per sample used in this study are provided in Table 1, with detailed U-Pb results given in Table DR1.<sup>1</sup>

### Analytical Methods

Zircon crystals were extracted from sediment samples by traditional methods of heavy mineral separation at the Arizona LaserChron

<sup>1</sup>GSA Data Repository item 2016026, U-Pb age distributions of samples, is available at <http://www.geosociety.org/pubs/ft2016.htm> or by request to [editing@geosociety.org](mailto:editing@geosociety.org).

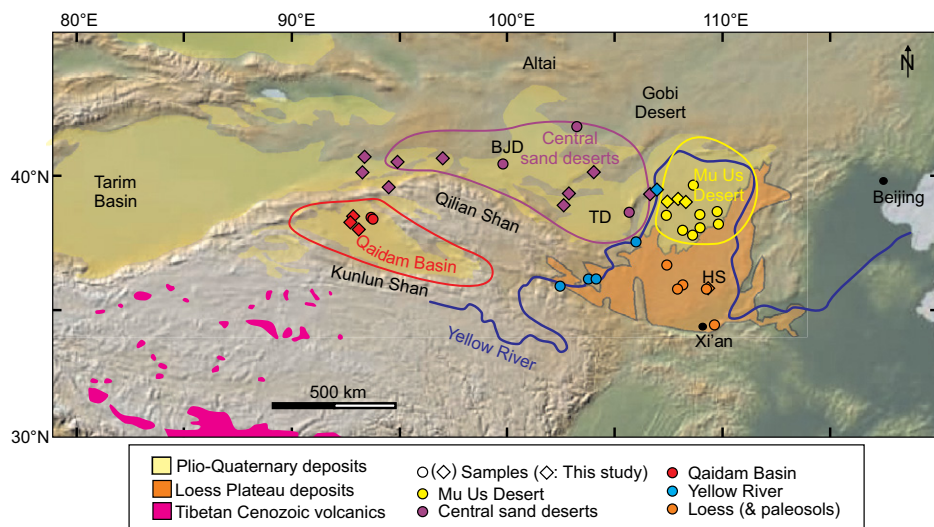


**Figure 2.** Map of central China displaying the four main potential source provinces for coarse eolian dust and the samples used in this study (nature of the samples detailed in Table 1). TD—Tengger Desert; BJD—Badan Jaran Desert; HS—Heimugou Section.

center (e.g., Gehrels et al., 2011). To minimize the hydraulic sorting grain-size effects and thus loss of fine-grained zircons in eolian dust samples, we used the recently developed ultrasonic separation technique of Hoke et al. (2014). Isotope ratios were measured using a Nu Plasma high-resolution (HR) multicollector–inductively coupled plasma–mass spectrometer (MC-ICP-MS) and a Thermo Element 2 single-collector (SC) ICP-MS coupled to a Photon Machines Analyte G2 193 nm excimer laser. Coarser-grained samples from the dust source areas were ablated using a 30  $\mu\text{m}$  laser beam diameter at 7.0 mJ (constant energy) with 94% laser energy at 7 Hz for the Nu Plasma and 8 Hz for the Element 2. Finer-grained samples (i.e., loess-paleosol) were analyzed using a 12  $\mu\text{m}$  beam diameter with same laser fluence and were analyzed on the Nu Plasma. Initial Pb was corrected using the  $^{204}\text{Pb}$  measurement and assuming an initial Pb composition from Stacey and Kramers (1975; see Table DR1 for more detail [footnote 1]). Note that the analyzed dust zircons have a minimum diameter of 12  $\mu\text{m}$  due to ICP-MS collector limitations, ion yields, and the Pb and U concentrations of the zircons. This resolution is nevertheless better than for previous eolian dust provenance studies, which commonly used laser spots  $>25 \mu\text{m}$  (e.g., Che and Li, 2013; Nie et al., 2014). Accordingly, the results presented in this study are valid for the eolian dust coarse fraction only. The origin of the finer fraction is beyond the focus of this study but has been discussed elsewhere (e.g., Derbyshire et al., 1998; Sun et al., 2006; Stevens and Lu, 2009).

### Assessing Sample-Size Effects

Provenance studies based on U-Pb age distributions of detrital zircons usually aim to identify all age components in samples of unknown provenance and compare them with the age components of known sources (Gehrels, 2000). To that end, 100–300 zircon ages per sample are commonly considered as a reasonable range to minimize the probability of failing to identify age components at low analytical cost (Vermeesch, 2004; Andersen, 2005).

The provenance problem that we face here is different, because all of the dominant age components are to some extent shared by the known eolian sources. Age distributions of the potential sources regions mainly differ in the relative contribution of four major age components: 225–330 Ma; 380–500 Ma; 750–1000 Ma; and 1500–2800 Ma (e.g., Gehrels et al., 2003; Stevens et al., 2010; Pullen et al., 2011; Lease et al., 2007, 2012; Weislogel et al., 2010). Previous provenance studies have attempted to distinguish among these contributions by comparing the relative magnitude of these age peaks in the age distribution of loess samples (Xiao et al., 2012; Nie et al., 2014). Although  $n = 100\text{--}300$  ages per sample are sufficient to ensure that each age component is found in the age distributions, these numbers are too low to constrain the relative contribution of each age peak (Pullen et al., 2014). As noted by Pullen et al. (2014), there is no minimum fixed number  $n$  that would completely stabilize the shape of the age distributions, but rather a range ( $n = 300\text{--}1000$ ), depending on the number of age groups present.

A good example of the uncertainty introduced by small  $n$  is shown in Figure 3. Subsamples made of randomly picked  $n = 100$  ages from a bigger sample of  $n = 928$  ages yield peak magnitudes that are different from each other as well as that of the larger- $n$  age population. Previous loess provenance studies comparing age peak magnitudes used samples with  $n$  commonly  $<300$  and have thus overinterpreted peak magnitude differences as real source differences, when in fact they may simply be due to scatter from the effects of subsampling. The same subsampling uncertainty also affects the MDS statistical technique of Vermeesch (2013) when applied to the loess provenance problem. The MDS produces a “map” of points, representing samples, on which the “distance” between points is related to the dissimilarity between samples, quantified by the KS statistic (Vermeesch and Garzanti, 2015). However, the KS statistic between two samples is based on the difference in their empirical distribution functions, the shape of which is controlled by subsampling as well (Massey, 1951). This uncertainty is illustrated in Figure 4. On the MDS plot, the random subsamples are widely scattered around the bigger sample, with some of them falling next to the Qaidam Basin age compilation, whereas others do not. Though MDS plots are an elegant way to visualize group differences when dealing with a huge number of samples, the distance between individual samples is influenced by subsampling variability and does not allow a quantitative estimate of the mismatch.

The age distributions of the 23 new individual samples are plotted in Figure 5. For all of them, main age peaks fit within the range of age peaks previously mentioned to be found in central China. However, the amplitude of age peaks in these individual samples, with  $n$  between 70 and 370, is expected to approximate but not perfectly characterize the “true” distribution of ages because of subsampling effects. To that end, the visualization and analysis of each sample age distribution are thus insufficient for solving our provenance problem. To minimize the uncertainty introduced by subsampling, our first step was to group individual samples into geographical provinces such that each province had a sufficiently large  $n$  number to increase the statistical significance of each age peak contribution ( $n$  between 800 and 2500). We divided the potential dust-source regions into four provenance provinces (Fig. 2):

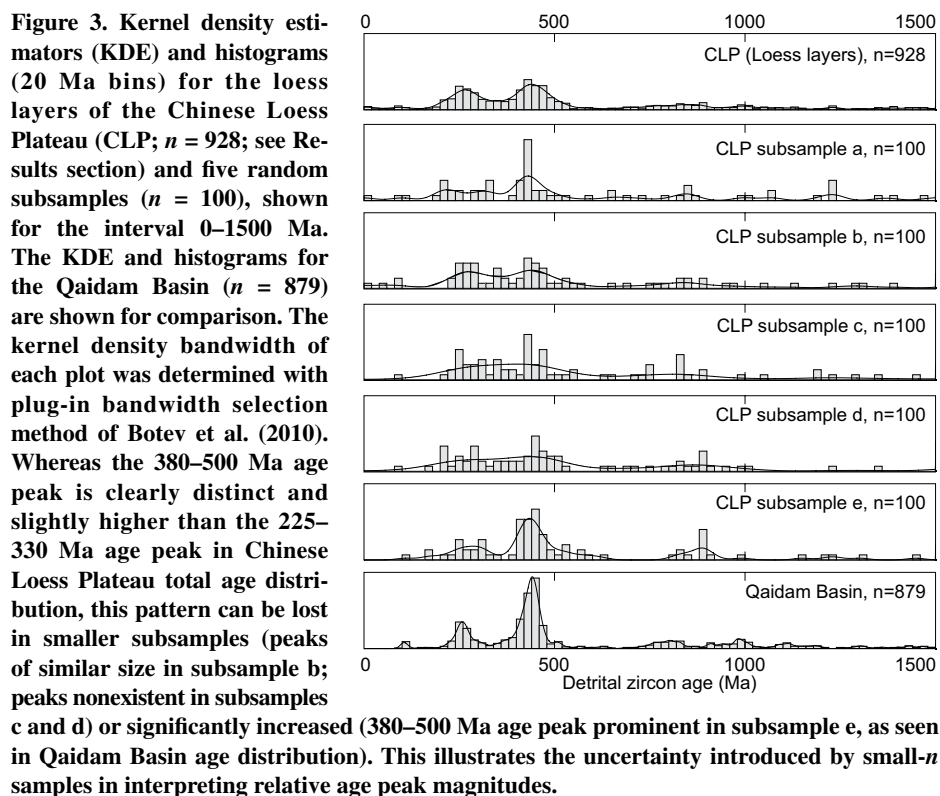
- (1) the sandy Mu Us Desert, located directly to the north of the Central Loess Plateau;
- (2) the central sand deserts, including both the Tengger and Badan Jaran Deserts, located to the northwest of the Chinese Loess Plateau,

TABLE 1. NATURE, LOCATION, AND NUMBER OF U-Pb AGES FOR THE SAMPLES USED IN THE STUDY

Sample name	n	Nature	Coordinates		Reference
			(°N)	(°E)	
<b>Mu Us Desert</b>					
13DUNE01	94	Eolian dune, Central Ordos Basin	38.98389	108.16321	This paper
13COSMO01	84	Top of yardang (Mesozoic sandstone)	38.9746	107.3386	This paper
13COSMO02	92	Top of yardang (Mesozoic sandstone)	38.972	107.343	This paper
13COSMO03	90	Top of yardang (Mesozoic sandstone)	39.1011	107.8649	This paper
MD10	98	Eolian dune, western Mu Us	37.9239	107.991	Stevens et al. (2013)
MD09	108	Eolian dune, western Mu Us	38.4923	107.227	Stevens et al. (2013)
MD08	119	Mesozoic eolian sandstone, eastern Mu Us	39.573	108.5151	Stevens et al. (2013)
MD07	93	Eolian dune, eastern Mu Us	38.6528	109.6644	Stevens et al. (2013)
MD06	58	Mesozoic eolian sandstone, eastern Mu Us	37.992	108.87	Stevens et al. (2013)
MD05	115	Quaternary fluvial deposits, eastern Mu Us	37.9871	108.822	Stevens et al. (2013)
MD04	74	Eolian dune, western Mu Us	37.706	108.488	Stevens et al. (2013)
MD03	113	Quaternary sand dune, western Mu Us	37.722	108.488	Stevens et al. (2013)
MD02	117	Eolian dune, eastern Mu Us	38.477	108.763	Stevens et al. (2013)
MD01	152	Eolian dune, eastern Mu Us	38.136	109.791	Stevens et al. (2010)
<b>Central deserts</b>					
13DUNE03	81	Eolian dune, Tengger Desert	40.07233	103.92398	This paper
13YARD01	82	Top of yardang, Badan Jaran Desert	40.5694	96.7546	This paper
13DUNE05	88	Eolian dune, Tengger Desert	39.28238	102.69492	This paper
13DUNE06	91	Eolian dune, Tengger Desert	38.80672	102.36845	This paper
13YARD02	66	Top of yardang, Badan Jaran Desert	40.48549	94.63945	This paper
TD1	86	Eolian dune, Tengger Desert	38.589	105.478	Stevens et al. (2010)
YG02	235	Fluvial sandstone, foothills of the Gobi-Altai Mountains	41.7	103.1	Che and Li (2013)
RSH01	230	Fluvial sandstone, Ruoshi River	40.4	99.6	Che and Li (2013)
13DUNE02*	82	Eolian dune, Tengger Desert	39.37441	106.5782	This paper*
13DUNE07*	94	Eolian dune, Yardang National Park	40.53599	93.10771	This paper*
13DUNE09*	90	Eolian dune, Yardang National Park	39.71717	94.35859	This paper*
13COSMO07*	84	Top of yardang (Pliocene–Quaternary sandstone)	40.53422	93.10758	This paper*
13COSMO09*	83	Top of yardang (Pliocene–Quaternary sandstone)	40.47707	93.13603	This paper*
<b>Qaidam Basin</b>					
10QBAP04	88	Quaternary alluvium	38.3	93.416667	Pullen et al. (2011)
MT226DZ6090	90	Pliocene–Quaternary lacustrine	38.3	93.416667	Pullen et al. (2011)
MT226DZ4060	92	Pliocene–Quaternary lacustrine	38.3	93.416667	Pullen et al. (2011)
MT226DZ0040	86	Pliocene–Quaternary lacustrine	38.3	93.416667	Pullen et al. (2011)
MT_97DZ4060	93	Pliocene–Quaternary lacustrine	38.3	93.416667	Pullen et al. (2011)
MT_97D2040	93	Pliocene–Quaternary lacustrine	38.3	93.416667	Pullen et al. (2011)
4–18–09–1	86	Top of yardang	38.2428	92.4412	This paper (see also Rohrmann et al., 2013)
4–17–09–1	90	Top of yardang	37.9667	92.7961	This paper (see also Rohrmann et al., 2013)
4–27–09–1	161	Top of yardang	38.3582	92.5104	This paper (see also Rohrmann et al., 2013)
<b>Northeast Tibet, Yellow River</b>					
13YELLOW01	367	River sediment	39.40816	106.7366	This paper
YR-1	121	River sediment	36.1388	103.609	Stevens et al. (2013)
CH12–21	118	River sediment	35.879167	102.22583	Nie et al. (2015)
YR-1	121	River sediment	36.139483	103.60908	Nie et al. (2015)
CH11YR03–04	321	River sediment	37.521967	105.66667	Nie et al. (2015)
YR-9C	108	River sediment	36.081139	103.86439	Nie et al. (2015)
<b>Loess deposits—Chinese Loess Plateau</b>					
HL1	84	Loess, Heimugou section	35.725883	109.06631	Pullen et al. (2011)
HL9	165	Loess, Heimugou section	35.725883	109.06631	Pullen et al. (2011)
HL15	239	Loess, Heimugou section	35.725883	109.06631	Pullen et al. (2011)
HL33	39	Loess, Heimugou section	35.725883	109.06631	Pullen et al. (2011)
XF-L1	90	Loess, Xifeng section	35.883	107.966	Xiao et al. (2012)
10YG-1	96	Loess, Weinan section	34.35	109.516	Xiao et al. (2012)
ljg	131	Loess, Xifeng section	35.78	107.78	Che and Li (2013)
LGM Loess	84	Loess, Huanxian section	36.6224	107.2867	Stevens et al. (2010)
<b>Paleosols—Chinese Loess Plateau</b>					
XF-S1	68	Paleosol, Xifeng section	35.883	107.966	Xiao et al. (2012)
10YG-2	88	Paleosol, Weinan section	34.35	109.516	Xiao et al. (2012)
TJZ-1	81	Paleosol, Xining section	36.45	101.783	Xiao et al. (2012)
slgj	261	Paleosol, Xifeng section	35.78	107.78	Che and Li (2013)
S-0	94	Paleosol, Heimugou section	35.725883	109.06631	This paper
S-1	108	Paleosol, Heimugou section	35.725883	109.06631	This paper
S-9	103	Paleosol, Heimugou section	35.725883	109.06631	This paper
S-15	105	Paleosol, Heimugou section	35.725883	109.06631	This paper
S-22	95	Paleosol, Heimugou section	35.725883	109.06631	This paper

Note: Global positioning system coordinates for samples from other studies, when not specified in their original publication, were estimated from published maps.

\*Samples have not been included in the regional clusters because either their location is at the interface between two clusters (sample 13DUNE02), or because they are located too far from the major dust-storm tracks supplying the Chinese Loess Plateau (see Figs. 1 and 2).



extending from the Qilian Mountains in the south to the Altai Mountains in the north;

(3) the Qaidam Basin, located to the west of the Chinese Loess Plateau and bounded by the Nan-Qilian, Altyn, and Kunlun mountains to the northeast, northwest, and south, respectively; and

(4) the Upper Yellow River drainage system in northeast Tibet, which transports sediment to the north of the Chinese Loess Plateau that can

be reworked by wind (Stevens et al., 2013; Nie et al., 2015).

These four provinces are considered to be the only direct providers of coarse-grained dust. A contribution from the Taklimakan and Gobi Deserts, located further west and north, has also been proposed (Che and Li, 2013; Nie et al., 2014; Yan et al., 2014). However, we argue that any coarse ( $>12 \mu\text{m}$ ) eolian zircon supply from these regions would have to transit via saltation

across the Mu Us, central sand deserts, and/or the Qaidam Basin and that its signature should be represented in the zircons of these three regions (Amit et al., 2014).

For the four selected source province regions, we compiled previously published and our new U-Pb zircon ages from eolian, fluvial, and lacustrine deposits, as well as from wind-eroded strata (see Table 1 for data compilation). All the selected U-Pb ages come either from Pliocene–Quaternary deposits, or from older strata (Miocene to Cretaceous) that exhibit evidence of having been wind eroded.

Note that five new samples were not incorporated in these four regional clusters (Table 1), because they are located either too far from the Chinese Loess Plateau, in areas characterized by easterly surface winds blowing into the Taklimakan (samples 13DUNE07, 13DUNE09, 13COSMO07, and 13COSMO09), or at the geographical boundary between two provenance provinces (sample 13DUNE02).

We divided the dust deposits of the Chinese Loess Plateau into two main groups:

(1) the Quaternary loess sequences, commonly numbered from L1 to L33 (younger to older), which were deposited during glacial periods (An et al., 1990); and

(2) the paleosol layers, numbered from S0 to S32, which experienced pedogenesis during interglacial periods (An et al., 1990; Porter and An, 1995).

For these two groups, we compiled new and existing U-Pb ages from samples located on the south and eastern parts of the Chinese Loess Plateau, excluding localities that are proximal to the potential provenance provinces, in order to avoid local bias in supply (i.e., Che and Li, 2013; Xiao et al., 2012).

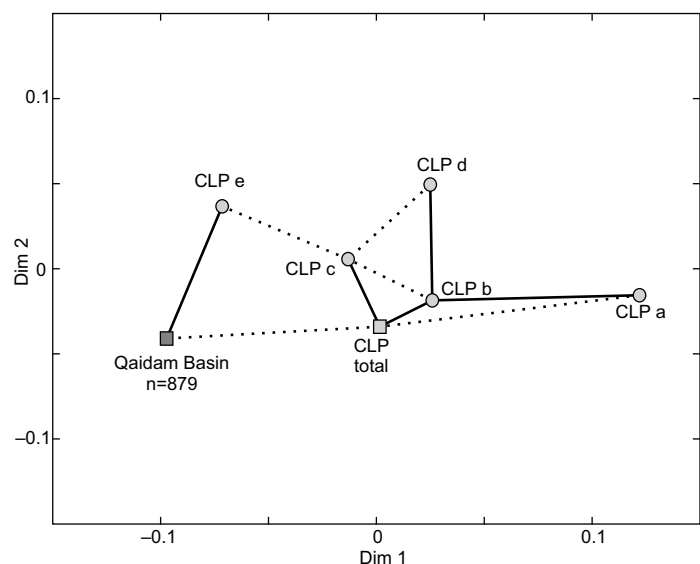


**Figure 4.** Multidimensional scaling (MDS) map for the loess layers of the Chinese Loess Plateau (CLP total), the five random subsamples of Figure 2, and Qaidam Basin. Axes are in dimensionless “KeS units” ( $0 < \text{Kolmogorov-Smirnov [KS]} < 1$ ) of dissimilarity between samples (Vermeesch, 2013). Solid lines and dashed lines connect samples with their “closest” and second-closest neighbors, respectively. Final “stress” value is 0.098, indicating a fit between “fair” and “good” (Vermeesch, 2013). Note that subsamples are randomly scattered around CLP total, with distances similar to the one separating Qaidam Basin and Chinese Loess Plateau age distributions. The uncertainty introduced here by subsampling does not allow these two areas to be distinguished.

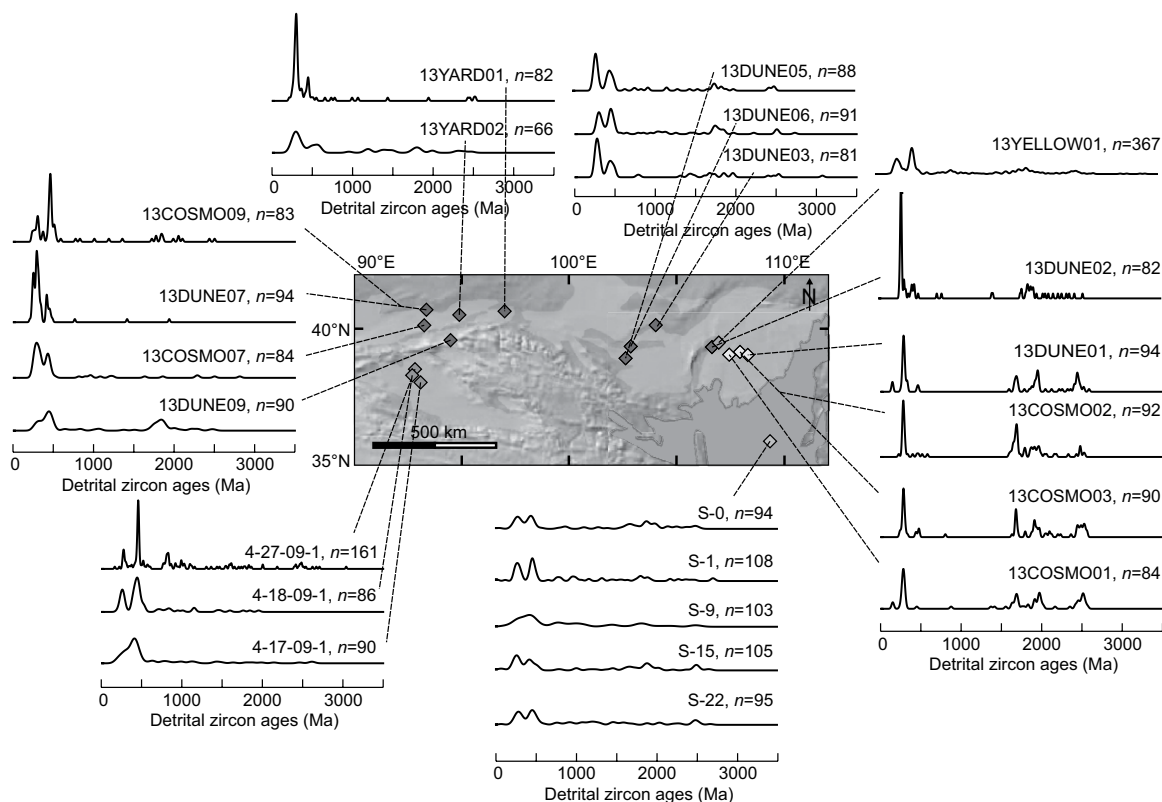


**Figure 5. Kernel density plots of the 23 samples presented in this study. The kernel density bandwidth of each plot was determined with plug-in bandwidth selection method of Botev et al. (2010). Same legend as Figure 2.**

### Statistical Analysis

The second step of our approach was to focus on the age distributions of the six geographical regions (the four provenance provinces and the two dust groups). The amplitudes of the age peak contributions are meaningful here given the large number of zircon ages ( $n > 800$ ) determined for each region. The age distributions can be visually compared using histogram diagrams, probability density plots (PDPs), and kernel density estimators (KDEs; Vermeesch, 2012). PDPs are omitted from the figures in this paper because KDE and PDP converge toward a single representation of the distribution of ages for large- $n$  data sets (Pullen et al., 2014). In an attempt to quantify sample age components and their contribution, we used the freeware BayesMix (Compston and Gallagher, 2012), which statistically determines the number, age, width, and contribution of individual components in age distributions. BayesMix uses a reversible jump Markov chain Monte-Carlo (RJ-MCMC) approach, which is an iterative, Bayesian sampling strategy that allows the number of individual components to change, as well as their age, width, and contribution, in order to best fit a given age distribution (Jasra et al., 2006; Gal-

agher et al., 2009). For each age data set used in the paper, BayesMix was run for 15,000 iterations (details in Table DR2 [see footnote 1]), assuming heavy skew- $t$  distributions with equal weighting on skewness.

One of the most promising attempts to quantitatively determine the contribution of different sources with complex age distributions in samples of unknown sourcing was provided by the iterative mixture modeling strategy of Amidon et al. (2005), and which was subsequently used on Tibetan samples (Lease et al., 2007, 2012). The iterative approach for mixture modeling of Amidon et al. (2005) consists of modeling synthetic age distributions by proportionally combining the probability density functions (PDFs) of the potential sources for the whole range of possible source combinations. Then, the best mixture is found by minimizing the dissimilarity between the synthetic PDFs and the PDF of the sample (or sets of samples in this case) of unknown sourcing, using the KS statistic or the areal percent mismatch as dissimilarity measures. This approach implies that the PDFs of each potential source region perfectly reflect the whole range of ages that contributes to the mixture. Erosion and sediment transport are nonstationary processes, however, and only

a small, random subsample of zircons from each source reaches the point of deposition. To take into account this potential variability in the zircon supply and the potential uncertainty introduced by random subsampling during erosion and transport, we developed a modified version of the strategy used by Amidon et al. (2005).

For each possible combination of the four identified source regions (for instance, Mu Us Desert: 20%, central sand deserts: 30%, Qaidam Basin: 12%, and northeast Tibet: 38%), we modeled  $N$  synthetic age distributions of 800 ages by randomly picking the necessary amount of ages in each source data set.  $N$  was chosen to be large enough to reproduce the potential variability in zircon subsampling. We then calculated the dissimilarity between each of these  $N$  synthetic age distributions and the loess (or paleosol) age distribution. There are different ways to determine the combinations that best fit the loess (or paleosol). A first approach is to determine the minimum dissimilarity value  $\delta_{\min}$  among the  $N$  synthetic age distributions and for the whole array of potential source combinations. The combinations that best fit the loess (or paleosol) are those for which this minimum  $\delta_{\min}$  value is reached for at least one of their  $N$  synthetic distributions. A second approach

is to consider the average dissimilarity value among the  $N$  synthetic age distributions per potential source combination. The combinations that best fit the loess (or paleosol) are those for which this average dissimilarity value is the lowest (named here  $\Delta_{\min}$ ). This way of determining the best fit takes into account the reproducibility of the dissimilarity values per source combination but minimizes the potential effect of subsampling in the contribution of the source provinces. A final approach is to consider the range of source combinations for which more than half (or two thirds, depending on the required precision) of the  $N$  synthetic distributions are “statistically similar” to the loess (or paleosol) age distribution. The notion of “statistical similarity” depends on the chosen dissimilarity measure.

We used the KS statistic as the dissimilarity measure, which has been shown to be an effective dissimilarity indicator (Vermeesch, 2013). We also tried another dissimilarity measure, the Anderson-Darling statistic, and it yielded no significant impact on the results (not shown).  $N = 200$  was recognized to be sufficient to stabilize the average dissimilarity values and their standard deviation. Two age distributions are considered statistically identical when the two-sample KS statistic does not reject the null hypothesis at the 95% confidence level.

## RESULTS AND INTERPRETATION

### U-Pb Age Distributions

Probability density plots, age histograms, and main age components for the maximum posterior models determined by the RJ-MCMC approach for the six geographic provinces are displayed in Figure 6. Mean, mode, standard deviation, and skew parameters for all components are given in Table DR2 (see footnote 1). Note that age components in the maximum posterior models are overall Gaussian, and that only the old (older than 1500 Ma) components display skewed distributions. Cumulative probability plots are shown in Figure 7.

The age distributions of the four potential provenance regions and loess and paleosol layers share several similar features. Grains younger than 700 Ma contribute from 40% (in the Mu Us Desert) to 60% (Qaidam Basin, northeast Tibet), and up to 70% (in the central sand deserts) of the total populations (Fig. 7). These young grains are divided into two major populations, centered at 240–270 Ma and 440–480 Ma, with relatively narrow distributions ( $1\sigma < 20$  Ma). Older grains are grouped into three main populations with wider distributions ( $1\sigma$  commonly  $> 50$  Ma), centered at 750–1130 Ma,

at 1645–1980 Ma, and 2430–2640 Ma, contributions of which vary from 2% to 25% of the total distributions.

Several distinctions can be made between the northern (Mu Us and central sand deserts) and southwestern provinces (Qaidam Basin and Upper Yellow River drainage system), as well as among individual regions:

(1) In the two northern provinces, the 240–270 Ma age peak is prominent (28%–48% of the total grains) and contributes twice as much as the 440–480 Ma age peak to the total age population. In contrast, the 440–480 Ma age peak is prominent in the southwestern provinces (30%–46% of the total grains). The 440–480 Ma age peak contributes ~25% more than the 240–270 Ma age peak to the total age population in Upper Yellow River sediment, and almost three times more in the Qaidam Basin.

(2) The zircon population centered at 750–1130 Ma is particularly important in the Qaidam Basin (~20%) and in Upper Yellow River sediment (~16%), and almost nonexistent in the northern provinces (2%–5%).

(3) The Mu Us Desert is distinguishable in having a large contribution (~60%) of grains older than 1500 Ma, whereas this contribution is less in other regions (~30%).

The age distributions of Yellow River, loess, and paleosol layers do not show any significant difference, and the contributions of major age peaks vary by only 2%–5% between the three distributions. The two-sample KS test between loess and paleosol layers yields a high  $P$  value ( $P = 0.86$ ), indicating that both distributions are statistically indistinguishable; this  $P$ -value is lower between Yellow River and loess ( $P = 0.18$ ) and between Yellow River and paleosol layers ( $P = 0.65$ ), though still indicating statistical similarity between age distributions. Grains younger than 700 Ma contribute ~50% of the total population; the 440–480 Ma age peak contributes 17%–32% more than the 240–270 Ma age peak to the total age population. The zircon population centered at 750–1130 Ma is important and contributes between 11% and 16%. Zircons older than 1500 Ma constitute the remaining 30% of the total age population. Note that Yellow River, loess, and paleosol layers yield a minor (1%–4%) population of very young grains (younger than 65 Ma), already noted by Pullen et al. (2011), that is absent in the three other potential provenance regions.

### Qualitative Assessment of Eolian Dust Provenance

The prominence of the 440–480 Ma age population in eolian dust samples compared to the 240–270 Ma age population (17%–32% higher)

is consistent with Upper Yellow River and/or Qaidam Basin being dominant sources. Statistical and visual similarity between loess or paleosol layers and Yellow River sediment indicates that the latter is likely the prominent source. However, minor contributions of coarse-grain zircon crystals from other provinces cannot be rejected if they are combined. Contributions of Upper Yellow River main age peaks appear to be intermediate between those of the Qaidam Basin and those of the two northern provinces. A combined contribution of both these regions could potentially result in a mixed age distribution that is similar to those of Yellow River sediment. We conclude that the eolian dust age distributions reflect a prominent contribution from the Yellow River, with a potential, minor additional supply from the three other provinces that is challenging to assess visually.

### Quantitative Assessment of Eolian Dust Provenance

We used the mixture modeling strategy introduced in Methods section to determine the combination of the four potential source regions that best fits the age distributions of loess and paleosol layers. The average dissimilarity to the loess and paleosol layers is displayed in ternary diagrams spanning the whole possible array of source combinations (Figs. 8 and 9). Combinations yielding the minimum dissimilarity value  $\delta_{\min}$  and lowest average dissimilarity value  $\Delta_{\min}$  are given in Table 2.

For loess layers, lowest average dissimilarity values (0.04–0.06) were obtained for a contribution of Qaidam Basin between 0% and 30%, contribution of the two northern provinces between 0% and 20% each, and a contribution of Yellow River sediment between 40% and 100% (Fig. 8). The range of combinations for which more than two thirds of the  $N$  random synthetic distributions are statistically similar to the loess is broader, with a Yellow River contribution that can decrease to 10%, mainly counterbalanced by an increasing contribution from Qaidam Basin. The minimum dissimilarity value  $\delta_{\min}$  and the lowest average dissimilarity  $\Delta_{\min}$  are relatively similar and indicate a best fit for a common contribution from the Yellow River of 58%–68%, a contribution from the Qaidam Basin between 14% and 20%, and the two northern provinces contributing the remainder.  $P$  values of the KS statistic for these combinations are  $>0.8$ , indicating a very good fit. These  $P$  values are higher than those for the KS test between Yellow River and loess age distributions.

The combinations that best fit the age distribution of paleosol layers are similar to those for

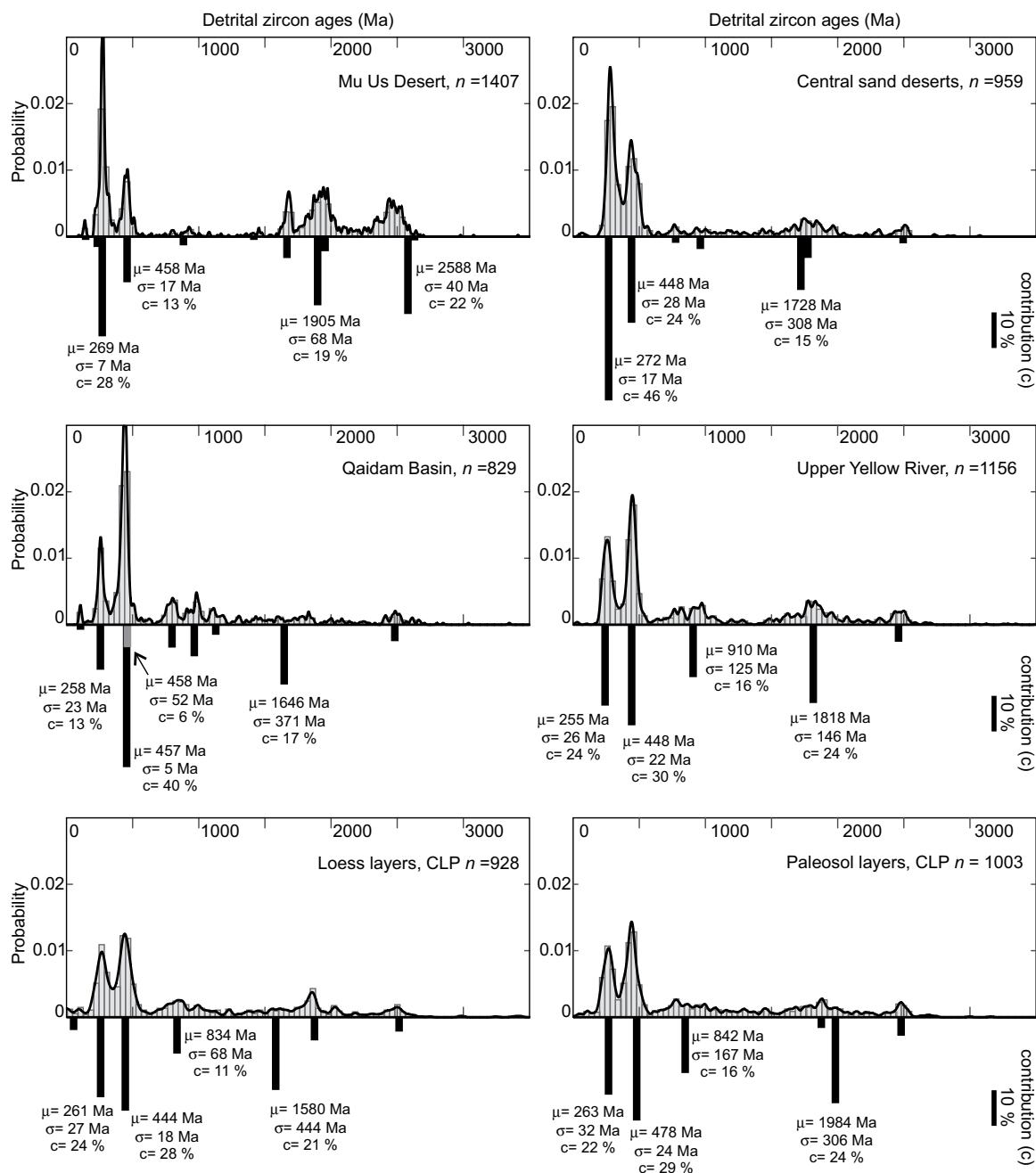


**Figure 6.** Normalized kernel density plots, histograms (40 Ma bins), and main components for the four potential source provinces (Mu Us Desert, central sand deserts, Qaidam Basin, and northeast Tibet), and the loess and paleosols layers of the Chinese Loess Plateau (CLP), shown for the interval 0–3500 Ma. Main components were obtained using the software BayesMix (see Methods section). The height of each vertical line reflects the component contribution (c) to the age population. Mean ( $\mu$ ) and standard deviation ( $\sigma$ ) are given for components with contribution  $>10\%$ . Note the juxtaposition of two components with similar mean age (457–458 Ma) but different standard deviations for the Qaidam Basin. Mean, mode, standard deviation, and skew parameters for all components are given in Table DR2 (see text footnote 1). Old (older than 1500 Ma) age peaks appear to be better resolved when slightly skewed in BayesMix maximum posterior models, explaining the visual offset between age peaks in density plots and components in several samples (peak at 2588 Ma for the Mu Us Desert).

the loess layers (Fig. 9). This is not surprising, considering the visual similarity between paleosol and loess age distributions. The minimum dissimilarity value  $\delta_{\min}$  indicates a best fit for a contribution from the Yellow River of 66%, a

contribution from the Qaidam Basin of 26%, and the two northern provinces contributing the remainder. The lowest average dissimilarity  $\Delta_{\min}$  is slightly different, indicating a best fit for a single provenance from the Yellow River (96%

of the total supply); however, other low average dissimilarity values (0.04–0.06) occupy a broad range similar to the one for loess layers.  $P$  values of the KS statistic for these combinations are also  $>0.8$ , indicating a very good fit.

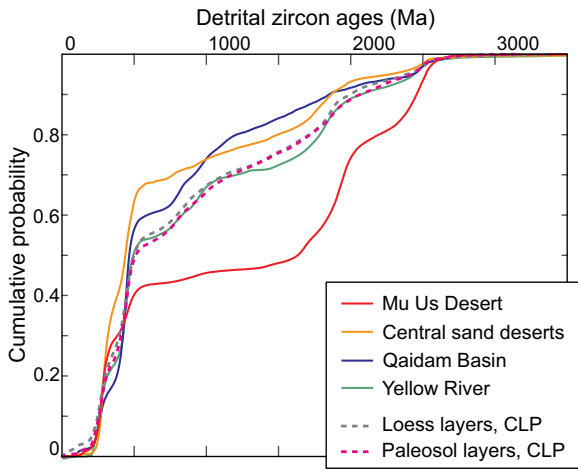


**Figure 7. Cumulative probability density plots for the four potential source provinces (Mu Us Desert, central sand deserts, Qaidam Basin, and upper Yellow River), and the loess and paleosols layers of the Chinese Loess Plateau (CLP), shown for the interval 0–3500 Ma.**

**DISCUSSION**

**Eolian Sedimentary Budget on the Chinese Loess Plateau**

Both visual and statistical assessments of eolian dust age distributions suggest that the Yellow River is the dominant source (>50%) for the coarse fraction of the eolian deposits of the Chinese Loess Plateau. Our statistical approach

also shows that dust age distributions are better explained with an additional, combined supply from the three other provinces, but not as significant as previously proposed (An et al., 1990; Ding et al., 1999; Pullen et al., 2011; Amit et al., 2014).

Our approach included mixing U-Pb data from various locations on the Chinese Loess Plateau to build large-*n* eolian dust U-Pb data sets. Thus, our analysis cannot address regional

variability in sediment sourcing on the loess plateau, which would be accomplished through analysis of single sample large-*n* data. In that sense, our results do not contradict previous U-Pb studies emphasizing the importance of the Mu Us Desert and the Yellow River as a major eolian source in the northern part of the Chinese Loess Plateau (Stevens et al., 2013; Bird et al., 2015; Nie et al., 2015), or northeast Tibet in its westernmost parts (Xiao et al., 2012; Che and Li, 2013; Bird et al., 2015). However, we argue that most of all the interpretations from previous U-Pb studies should be taken with caution because they are based on only 80–200 ages per sample (i.e., Stevens et al., 2010, 2013; Pullen et al., 2011; Xiao et al., 2012; Che and Li, 2013; Nie et al., 2014), and may thus be influenced by age subsampling effects (e.g., Fig. 3). Similarly, grouping U-Pb ages in regional clusters results in a loss of information on variation in the sediment composition in the source regions themselves. For instance, previous studies have emphasized variability of U-Pb age distributions within the Mu Us Desert, with western Mu Us sands showing a significant contribution from eolian recycling from Yellow River sediment (Stevens et al., 2010, 2013). Localized sourcing from more spatially limited areas cannot be

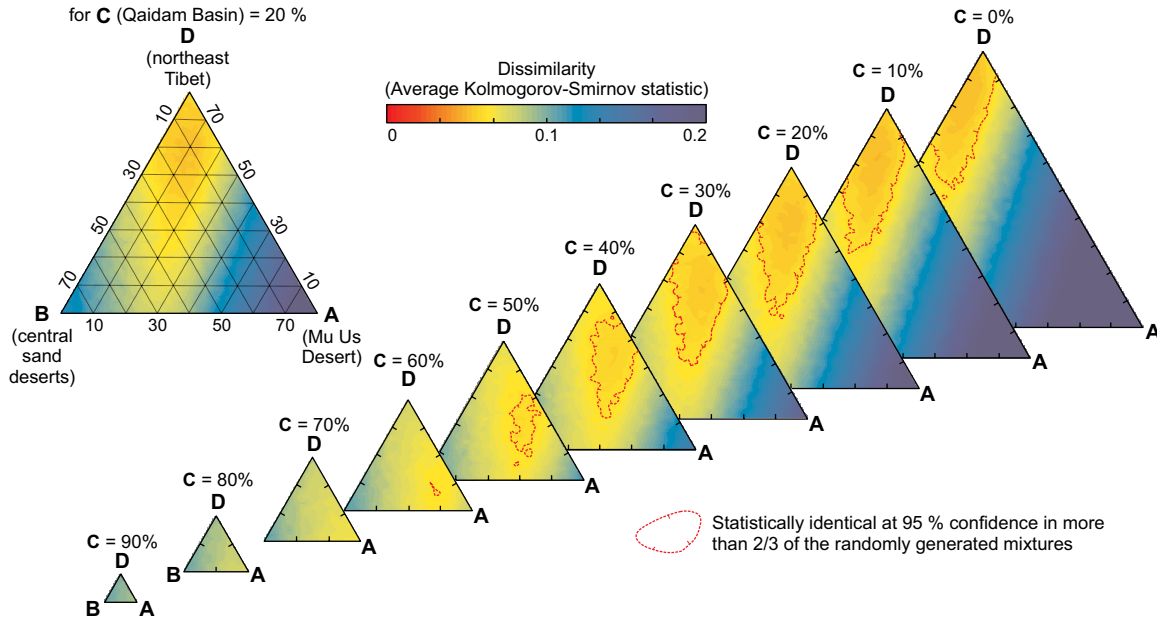


**Figure 8. Dissimilarity to the loess layers of the Chinese Loess Plateau for each possible combination of the four potential source regions (A—Mu Us Desert; B—central sand deserts; C—Qaidam Basin; D—upper Yellow River). Each triangle is a ternary diagram of contribution from the provinces A, B, and D for a given contribution of C (contributions of A + B + C + D = 100% for each triangle; see example for C = 20% on the left side of the figure). The color bar indicates the range of values for the dissimilarity measure, here the Kolmogorov-Smirnov (KS) statistic averaged for *N* random synthetic distributions per source combination (*N* = 200). The combinations that best fit the loess age distribution are the ones that give the lowest dissimilarity values. An alternative way to determine the best fit is to look at the range of combinations for which more than two thirds of the *N* random synthetic distributions are statistically similar to the loess (here in the sense of the KS statistic at the 95% confidence level), depicted by red isolines in the figure.**

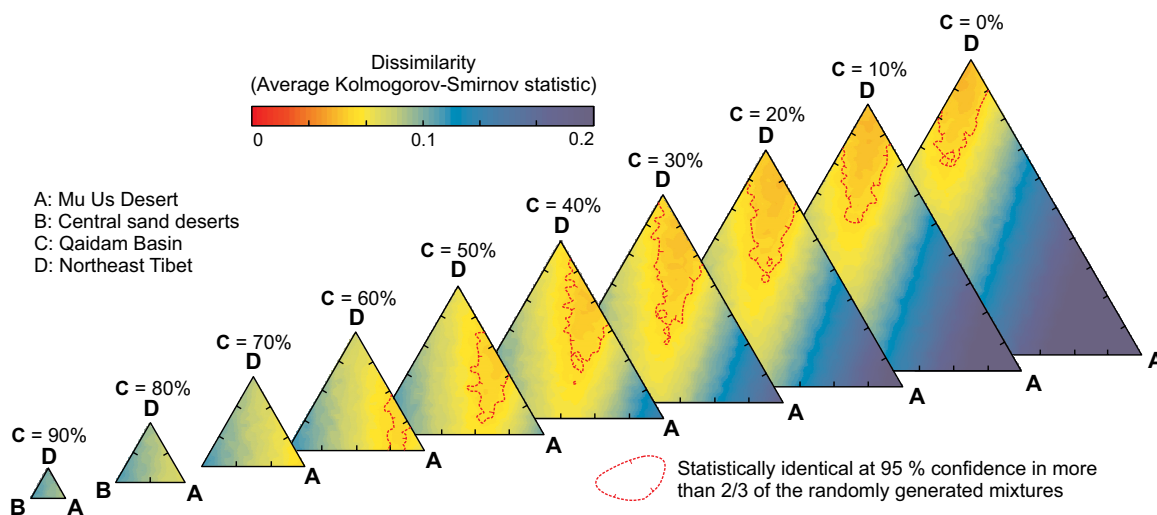


**Figure 9.** Dissimilarity to the paleosol layers of the Chinese Loess Plateau for each possible combination of the four potential source regions. Same legend as Figure 8 (A—Mu Us Desert; B—central sand deserts; C—Qaidam Basin; D—upper Yellow River).

investigated with our methodology and current data set, but it is likely that the continuously increasing number of U-Pb data from central China will allow it in the near future. In this regard, our study is valuable because it provides an approach about how to assess these increasingly large-*n* data sets. Finally, it is important to remember that we only investigated a fraction of the provenance signal by using U-Pb ages of “coarse” zircons (laser spot diameter of 12 μm for dust samples; 30 μm otherwise). Relative contribution estimates may change significantly when smaller grain sizes are considered.

Our eolian budget estimates confirm that Yellow River input buffers the contribution of other sources to the Chinese Loess Plateau for the dust coarse fraction (Stevens et al., 2013; Nie et al., 2015). This prominent contribution is corroborated by heavy mineral counting, framework petrography, and sediment flux estimates (Nie et al., 2015). These results do not completely rule out other modes of transportation for the Tibetan-sourced dust, because they cannot tell the difference between zircons that came from Tibet via the Yellow River and were then reworked by winds further north (Stevens et al., 2013; Nie et al., 2015), and zircons that were blown directly off the Yellow River drainage basin and landed on the Chinese Loess Plateau (Pullen et al., 2011). They do, however, corroborate minor yet significant supply of coarse sediment from the Qaidam Basin (Pullen et al., 2011; Kapp et al., 2011). The range of potential Qaidam Basin contribution that could best explain the dust age distributions is yet relatively broad—and thus uncertain—in our statistical estimates (Figs. 8 and 9). This

is not surprising, because Qaidam Basin and Yellow River age distributions are relatively similar, in contrast to the age distributions of the two northern provinces. This is partly due to the fact that parts of the Yellow River source tributaries drain northern Tibet and the Kunlun Mountains, areas that also bound and supply the Qaidam Basin (Yin et al., 2008). Given the importance of large *n* to distinguish both provinces, it is likely that their relative contributions to the eolian budget will continue to change as more data are generated. Our results yet corroborate the existence of an alternative dust-storm pathway through the Qaidam Basin, infrequent today but that must have been active in the past (Vandenberghe et al., 2006; Kapp et al., 2011; Pullen et al., 2011; Rohrmann et al., 2013). Eolian erosion in the Qaidam Basin has been interpreted to be most significant during glacial periods (Kapp et al., 2011; Rohrmann et al., 2013). In this regard, a notable finding is the lack of a detectable difference in sourcing between glacial (loess) and interglacial (paleosols) deposits. Constant Yellow River contribution during both periods is not surprising because fluvial reworking should have occurred regardless of most

changes in atmospheric circulation, as Yellow River fluvial sediment surrounds the Chinese Loess Plateau to the west and north (Nie et al., 2015). However, minor Qaidam Basin contribution to the eolian supply during interglacials is counterintuitive, because modern dust-storm outbreaks are very limited there (Sun et al., 2001). An explanation for this minor Qaidam component in paleosol layers is that part of the interglacial dust is also recycled from previous glacial (and interglacial) deposits (Kohfeld and Harrison, 2003; van Loon, 2006; Kapp et al., 2015). Eolian dust recycling in loess accumulations has been shown to be a significant process in other areas (e.g., Mroczek, 2013; Sweeney and Mason, 2013). Extensive sediment reworking by wind would serve to homogenize the composition of glacial-aged loess and dust in interglacial-aged paleosols.

We thus suspect that the relative contribution of the northern and northwestern deserts compared to the Qaidam Basin was more important during interglacials, such as observed today (Wang et al., 2004), but this contribution has been significantly dampened by recycling of older loess. Similarly, the relative contribution from the Qaidam Basin during glacials was

TABLE 2. COMBINATIONS YIELDING MINIMUM DISSIMILARITY VALUE  $\Delta_{\text{MIN}}$  AND LOWEST AVERAGE DISSIMILARITY VALUE  $\delta_{\text{MIN}}$

	Loess layers		Paleosol layers	
	Minimum dissimilarity value, $\delta_{\text{min}}$ (%)	Average dissimilarity value, $\Delta_{\text{min}}$ (%)	Minimum dissimilarity value, $\delta_{\text{min}}$ (%)	Average dissimilarity value, $\Delta_{\text{min}}$ (%)
Mu Us Desert	8	6	6	0
Central sand deserts	14	12	2	4
Qaidam Basin	20	14	26	0
Northeast Tibet	58	68	66	96

likely greater than during interglacials, and this proportion has been reduced by reworking of older deposits.

### “Eolian Cannibalism” and the Building of the Chinese Loess Plateau

Our contribution estimates imply that buffering of dust supply by reworking of Yellow River sediment and intense reworking of older loess and paleosol deposits have served to mix eolian dust and homogenize their provenance signatures. This explanation is supported by similar heavy mineral assemblages for both loess and paleosol layers (Nie and Peng, 2014). It is also corroborated by recent geomorphological analyses of wind erosion features in the Mu Us Desert and on the northern part of the Chinese Loess Plateau, suggesting that the central and eastern Loess Plateau previously extended farther to the north and west of its modern windward escarpment, and that this extension has been reworked and redeposited further south during the late Quaternary (Kapp et al., 2015). Considering that eolian dust accumulation rates were commonly 2–20 times larger during glacial periods than during interglacial periods, with a high regional variability (Kohfeld and Harrison, 2003; Sun et al., 2008), it is not surprising that recycling on the Chinese Loess Plateau homogenized eolian zircon populations toward glacial conditions, with a significant Qaidam Basin (~20%) contribution.

These findings corroborate the idea that the Chinese Loess Plateau is a dynamic landform where deflation, lateral transport by winds and rivers, and aggradation are equally important (Nie et al., 2015; Kapp et al., 2015). Evidence of extensive reworking of fluvial and eolian sediment suggests that the extensive Quaternary loess sequences are just the tip of the iceberg of a much longer accumulation history. Older, pre-Quaternary loess deposits at the margin of the Chinese Loess Plateau are likely to have been cannibalized by winds, such as seen in the Mu Us Desert (Kapp et al., 2015), or reworked by fluvial processes and redeposited, leaving a few isolated remnant deposits (An et al., 2001; Guo et al., 2002; Alonso-Zarza et al., 2009; Licht et al., 2014).

Evidence of intense recycling and “over-representation” of Yellow River sediment and glacially sourced dust raise concerns about the relevance of several paleoclimatic proxies applied to Chinese loess sequences. Petrography, mineralogy, or geochemistry analyses of single-particle or bulk eolian sediment might be significantly either buffered by fluvial provenance and/or biased toward glacial dust, explaining why many studies found changes of sediment properties between loess and paleo-

sol layers to be much weaker compared to the regional variability (e.g., Gylesjö and Arnold, 2006; Jeong et al., 2011; Yan et al., 2014; Nie and Peng, 2014). We suggest that proxies linked to in situ pedogenic development (in contrast with proxies linked to basinwide pedogenic development, as dust fine-fraction clay-mineralogy, likely related to weathering in the sediment source areas) are the only ones lacking bias toward glacial conditions and fluvial sediment reworking because they are independent of sediment sourcing. Notably, iron-oxide mineralogy, as well as magnetic susceptibility and other various magnetic parameters, have been shown to highlight significant differences between loess and paleosol layers (e.g., Maher and Thompson, 1991; Deng et al., 2004; Song et al., 2014). This can be explained by the overall authigenic character of magnetic minerals, which form in situ in paleosol layers rather than being transported by winds (e.g., Maher and Thompson, 1991, and references therein). However, recycling of pedogenic microstructures, including clay aggregates and iron-oxide nodules, has been shown to be significant in other loess accumulations (Mroczek, 2013). In that sense, paleoclimatic proxies linked to in situ pedogenic development might be biased to a small degree by the reworking of older Chinese paleosol layers as well, though this assumption is hard to verify.

### Implications for the Genesis of the Chinese Loess Plateau

Our findings emphasize the prominent role of eolian reworking of freshly brought fluvial sediment and older loess deposits in the building of the Chinese Loess Plateau. We thus suspect that two distinct phenomena might have controlled the recent Pliocene–Quaternary increase as well as the long-term Cenozoic increase in eolian accumulation rates (Sun et al., 2008, 2011).

First, increased denudation of northeast Tibet and consecutive fluvial transport further north must have significantly enhanced loess accumulation (Nie et al., 2015). Active deformation and resultant rock uplift have modified the topography and increased denudation of the northeastern margin of Tibet throughout the Cenozoic, with a recent acceleration since the middle-late Miocene (e.g., Métivier et al., 1998; Clark et al., 2010; Duvall et al., 2011; Li et al., 2011; Lease et al., 2012). Increased erosion due to the onset of oscillating glacial conditions (Peizhen et al., 2001) and the setup of the Yellow River in its modern course (Craddock et al., 2010; Nie et al., 2015) must have additionally increased fluvial sedimentary input into the Chinese Loess Plateau and its consecutive reworking by winds.

Moreover, we suspect that increased eolian accumulation rates might reflect enhanced recycling of older loess and fluvial strata as much as increased dust generation. Indeed, the long-term erosion of older eolian and fluvial strata and their recycling in younger eolian dust deposits should reduce the spatial extent and thickness of older loess deposits, whereas younger loess deposits would appear prominent in the fossil record. It is thus very likely that changes in accumulation rates or regional onsets of eolian sedimentation in the fossil record are strongly biased by this recycling effect. Note that we do not question the numerous other paleoclimatic proxy records demonstrating aridification and desert expansion since the late Miocene (e.g., Wang et al., 1999; Wang et al., 2006; Wu et al., 2007; Han et al., 2014). However, we suspect that increasing aridity throughout the Pliocene–Quaternary might have favored the reworking of older deposits on the Chinese Loess Plateau as much as dust generation in distant deserts.

### CONCLUSION

Our study highlights how provenance interpretations based on U–Pb ages of detrital zircons can be misleading when based on a small number of zircon ages. As already emphasized previously (Pullen et al., 2014), we argue that interpretations based on age peak heights, as well as mixture modeling of provenance provinces, are only meaningful when the number of ages per region is high enough (here >800) to stabilize the shape of age distributions. We present a new mixture modeling method to quantify the contribution of different sources of known age distribution. Our method takes into account the potential uncertainties introduced by random zircon subsampling during erosion and transport and allows us to statistically estimate the combination of known sources that best fits the age distribution of samples of unknown sourcing.

Our contribution estimates based on available data indicate that the coarse eolian dust sedimentary budget on the Chinese Loess Plateau is dominated by Yellow River–brought sediment (60%–70%). These results emphasize the importance of recycling of fluvial deposits in the loess sedimentary budget. Moreover, our findings confirm minor Qaidam Basin input (~20%) and thus support the existence of an alternative dust-generating storm pathway through the Qaidam Basin and northern Tibetan Plateau, likely active during past glacial and possibly stadial periods. In this regard, the lack of a significant difference in sourcing between glacial (loess) and interglacial (paleosols) deposits is particularly noteworthy. This implies that intense reworking of older loess and paleosol

deposits has additionally served to mix eolian dust and homogenize their provenance signatures. Our findings corroborate the idea that the Chinese Loess Plateau is a dynamic landform where wind deflation, lateral transport by wind and rivers, and aggradation are equally important. Moreover, they suggest that paleoclimatic interpretations based on loess accumulation rates or on eolian dust features might be significantly biased by these recycling effects. Finally, we propose that a significant part of the older, pre-Quaternary deposits surrounding the Chinese Loess Plateau might have been partly cannibalized and recycled in more recent loess deposits following increasing regional aridity throughout the Pliocene–Quaternary.

#### ACKNOWLEDGMENTS

This research was primarily funded by the U.S. National Science Foundation (NSF grants AGS-1203973 and AGS-1203427). Licht was also funded by a Fyssen Foundation study grant (2014), Kansas University (2015), and Marie Curie fellowship ECAMMETT 656731 (2015–2016). We also acknowledge NSF grant EAR 1338583 for support of the Arizona LaserChron Center. We thank H. Chang, N. Mclean, A. Möller, K. Gallagher, K.C. Beard, M. Pecha, G. Simpson, I. Nurmaya, and C. White for sample collection, prolific discussions, and assistance in the laboratory.

#### REFERENCES CITED

- Alonso-Zarza, A., Zhao, Z., Song, C., Li, J., Zhang, J., Martín-Pérez, A., Martín-García, R., Wang, X., Zhang, Y., and Zhang, M., 2009, Mudflat/distal fan and shallow lake sedimentation (upper Vallesian–Turolian) in the Tianshui Basin, central China: Evidence against the late Miocene eolian loess: *Sedimentary Geology*, v. 222, p. 42–51, doi:10.1016/j.sedgeo.2009.03.010.
- Amidon, W., Burbank, D., and Gehrels, G., 2005, U-Pb zircon ages as a sediment mixing tracer in the Nepal Himalaya: *Earth and Planetary Science Letters*, v. 235, p. 244–260, doi:10.1016/j.epsl.2005.03.019.
- Amit, R., Enzel, Y., Mushkin, A., Gillespie, A., Batbaatar, J., Crouvi, O., Vandenberghe, J., and An, Z., 2014, Linking coarse silt production in Asian sand deserts and Quaternary accretion of the Chinese Loess Plateau: *Geology*, v. 42, p. 23–26, doi:10.1130/G34857.1.
- An, Z., Tunghseng, L., Yanchou, L., Porter, S.C., Kukla, G.H.W.X., Xihao, W., and Yingming, H., 1990, The long-term paleomonsoon variation recorded by the loess-paleosol sequence in central China: *Quaternary International*, v. 7, p. 91–95.
- An, Z., Kutzbach, J., Prell, W., and Porter, S., 2001, Evolution of Asian monsoons and phased uplift of the Himalaya–Tibetan Plateau since late Miocene times: *Nature*, v. 411, p. 62–66, doi:10.1038/35075035.
- Andersen, T., 2005, Detrital zircons as tracers of sedimentary provenance: Limiting conditions from statistics and numerical simulations: *Chemical Geology*, v. 216, p. 249–270, doi:10.1016/j.chemgeo.2004.11.013.
- Bird, A., Stevens, T., Rittner, M., Vermeesch, P., Carter, A., Andò, S., Garzanti, E., Lu, H., Nie, J., Zeng, L., Zhang, H., and Xu, Z., 2015, Quaternary dust source variation across the Chinese Loess Plateau: *Palaeogeography, Palaeoclimatology, Palaeoecology*, v. 435, p. 254–264, doi:10.1016/j.palaeo.2015.06.024.
- Botev, Z.I., Grotowski, J.F., and Kroese, D.P., 2010, Kernel density estimation via diffusion: *Annals of Statistics*, v. 38, p. 2916–2957, doi:10.1214/10-AOS799.
- Che, X., and Li, G., 2013, Binary sources of loess on the Chinese Loess Plateau revealed by U-Pb ages of zircon: *Quaternary Research*, v. 80, p. 545–551, doi:10.1016/j.yqres.2013.05.007.
- Clark, M.K., Farley, K.A., Zheng, D., Wang, Z., and Duvall, A.R., 2010, Early Cenozoic faulting of the northern Tibetan Plateau margin from apatite (U-Th)/He ages: *Earth and Planetary Science Letters*, v. 296, p. 78–88, doi:10.1016/j.epsl.2010.04.051.
- Compston, W., and Gallagher, K., 2012, New SHRIMP zircon ages from tuffs within the British Palaeozoic stratotypes: *Gondwana Research*, v. 21, p. 719–727, doi:10.1016/j.gr.2011.11.010.
- Craddock, W.H., Kirby, E., Harkins, N.W., Zhang, H., Shi, X., and Liu, J., 2010, Rapid fluvial incision along the Yellow River during headward basin integration: *Nature Geoscience*, v. 3, p. 209–213, doi:10.1038/ngeo777.
- Deng, C., Zhu, R., Verosub, K.L., Singer, M.J., and Vidic, N.J., 2004, Mineral magnetic properties of loess/paleosol couplets of the central loess plateau of China over the last 1.2 Myr: *Journal of Geophysical Research—Solid Earth*, v. 109, B01103, doi:10.1029/2003JB002532.
- Derbyshire, E., Meng, X., and Kemp, R.A., 1998, Provenance, transport and characteristics of modern aeolian dust in western Gansu Province, China, and interpretation of the Quaternary loess record: *Journal of Arid Environments*, v. 39, p. 497–516, doi:10.1006/jare.1997.0369.
- Ding, Z., Sun, J., Rutter, N.W., Rokosh, D., and Liu, T., 1999, Changes in sand content of loess deposits along a north-south transect of the Chinese Loess Plateau and the implications for desert variations: *Quaternary Research*, v. 52, p. 56–62, doi:10.1006/qres.1999.2045.
- Duvall, A.R., Clark, M.K., van der Pluijm, B.A., and Li, C., 2011, Direct dating of Eocene reverse faulting in northeastern Tibet using Ar-dating of fault clays and low-temperature thermochronometry: *Earth and Planetary Science Letters*, v. 304, p. 520–526, doi:10.1016/j.epsl.2011.02.028.
- Gallagher, K., Charvin, K., Nielsen, S., Sambridge, M., and Stephenson, J., 2009, Markov chain Monte Carlo (MCMC) sampling methods to determine optimal models, model resolution and model choice for earth science problems: *Marine and Petroleum Geology*, v. 26, p. 525–535, doi:10.1016/j.marpetgeo.2009.01.003.
- Gehrels, G.E., 2000, Introduction to detrital zircon studies of Paleozoic and Triassic strata in western Nevada and northern California, in Soreghan, M.J., and Gehrels, G.E., eds., *Paleozoic and Triassic Paleogeography and Tectonics of Western Nevada and Northern California*: Geological Society of America Special Paper 347, p. 1–17, doi:10.1130/0-8137-2347-7.1.
- Gehrels, G., Yin, A., and Wang, X., 2003, Detrital-zircon geochronology of the northeastern Tibetan Plateau: *Geological Society of America Bulletin*, v. 115, p. 881–896, doi:10.1130/0016-7606(2003)115<0881:DGOTNT>2.0.CO;2.
- Gehrels, G., Kapp, P., DeCelles, P., Pullen, A., Blakey, R., Weislogel, A., Ding, L., Guynn, J., Martin, A., McQuarrie, N., and Yin, A., 2011, Detrital zircon geochronology of pre-Tertiary strata in the Tibetan-Himalayan orogen: *Tectonics*, v. 30, TC5016, doi:10.1029/2011TC002868.
- Guo, Z., Ruddiman, W., Hao, Q., Wu, H., Qiao, Y., Zhu, R., Peng, S., Wei, J., Yuan, B., and Liu, T., 2002, Onset of Asian desertification by 22 Myr ago inferred from loess deposits in China: *Nature*, v. 416, p. 159–163, doi:10.1038/416159a.
- Gyölesjö, S., and Arnold, E., 2006, Clay mineralogy of a red clay-loess sequence from Lingtai, the Chinese Loess Plateau: *Global and Planetary Change*, v. 51, p. 181–194, doi:10.1016/j.gloplacha.2006.03.002.
- Han, W., Fang, X., Ye, C., Teng, X., and Zhang, T., 2014, Tibet forcing Quaternary stepwise enhancement of westerly jet and Central Asian aridification: Carbonate isotope records from deep drilling in the Qaidam salt playa, NE Tibet: *Global and Planetary Change*, v. 116, p. 68–75, doi:10.1016/j.gloplacha.2014.02.006.
- Hoke, G., Schmitz, M., and Bowring, S., 2014, An ultrasonic method for isolating nonclay components from clay-rich material: *Geochemistry Geophysics Geosystems*, v. 15, p. 492–498, doi:10.1002/2013GC005125.
- Jasra, A., Stephens, D., Gallagher, K., and Holmes, C., 2006, Bayesian mixture modelling in geochronology via Markov chain Monte Carlo: *Mathematical Geology*, v. 38, p. 269–300, doi:10.1007/s11004-005-9019-3.
- Jeong, G.Y., Hillier, S., and Kemp, R.A., 2011, Changes in mineralogy of loess-paleosol sections across the Chinese Loess Plateau: *Quaternary Research*, v. 75, p. 245–255, doi:10.1016/j.yqres.2010.09.001.
- Kang, S., Lu, Y.C., and Wang, X.L., 2011, Closely-spaced recuperated OSL dating of the last interglacial paleosol in the southeastern margin of Chinese Loess Plateau: *Quaternary Geochronology*, v. 6, p. 480–490, doi:10.1016/j.quageo.2011.04.004.
- Kang, S., Wang, X., and Lu, Y., 2013, Quartz OSL chronology and dust accumulation rate changes since the Last Glacial at Weinan on the southeastern Chinese Loess Plateau: *Boreas*, v. 42, p. 815–829.
- Kapp, P., Pelletier, J., Rohrmann, A., Heermance, R., Russell, J., and Ding, L., 2011, Wind erosion in the Qaidam Basin, Central Asia: Implications for tectonics, paleoclimate, and the source of the Loess Plateau: *GSA Today*, v. 21, p. 4–10, doi:10.1130/GSATG99A.1.
- Kapp, P., Pullen, A., Pelletier, J.D., Russell, J., Goodman, P., and Cai, F., 2015, From dust to dust: Quaternary wind erosion of the Mu Us Desert and Loess Plateau, China: *Geology*, v. 43, p. 835–838, doi:10.1130/G36724.1.
- Kohfeld, K., and Harrison, S., 2003, Glacial-interglacial changes in dust deposition on the Chinese Loess Plateau: *Quaternary Science Reviews*, v. 22, p. 1859–1878, doi:10.1016/S0277-3791(03)00166-5.
- Lease, R., Burbank, D., Gehrels, G., Wang, Z., and Yuan, D., 2007, Signatures of mountain building: Detrital zircon U/Pb ages from northeastern Tibet: *Geology*, v. 35, p. 239–242, doi:10.1130/G23057A.1.
- Lease, R., Burbank, D., Hough, B., Wang, Z., and Yuan, D., 2012, Pulsed Miocene range growth in northeastern Tibet: Insights from Xunhua Basin magnetostratigraphy and provenance: *Geological Society of America Bulletin*, v. 124, p. 657–677, doi:10.1130/B30524.1.
- Li, G., Pettko, T., and Chen, J., 2011, Increasing Nd isotopic ratio of Asian dust indicates progressive uplift of the north Tibetan Plateau since the middle Miocene: *Geology*, v. 39, p. 199–202, doi:10.1130/G31734.1.
- Licht, A., van Cappelle, M., Abels, H.A., Ladant, J., Trabucho-Alexandre, J., France-Lanord, C., Donnadiou, Y., Vandenberghe, J., Rigaudier, T., Lecuyer, C., Terry, D., Jr., Adriaens, R., Boura, A., Guo, Z., Aung Naing Soe, Dupont-Nivet, G., and Jaeger, J.-J., 2014, Asian monsoons in a late Eocene greenhouse world: *Nature*, v. 513, p. 501–506, doi:10.1038/nature13704.
- Maher, B.A., and Thompson, R., 1991, Mineral magnetic record of the Chinese loess and paleosols: *Geology*, v. 19, p. 3–6, doi:10.1130/0091-7613(1991)019<0003:MMROC>2.3.CO;2.
- Massey, F.J., Jr., 1951, The Kolmogorov-Smirnov test for goodness of fit: *Journal of the American Statistical Association*, v. 46, p. 68–78, doi:10.1080/01621459.1951.10500769.
- Métivier, F., Gaudemer, Y., Tapponnier, P., and Meyer, B., 1998, Northeastward growth of the Tibet Plateau deduced from balanced reconstruction of two depositional areas: The Qaidam and Hexi Corridor basins, China: *Tectonics*, v. 17, p. 823–842, doi:10.1029/98TC02764.
- Mroczek, P., 2013, Recycled loesses—A micromorphological approach to the determination of local source areas of Weichselian loess: *Quaternary International*, v. 296, p. 241–250, doi:10.1016/j.quaint.2013.02.040.
- Nie, J., and Peng, W., 2014, Automated SEM-EDS heavy mineral analysis reveals no provenance shift between glacial loess and interglacial paleosol on the Chinese Loess Plateau: *Aeolian Research*, v. 13, p. 71–75, doi:10.1016/j.aeolia.2014.03.005.
- Nie, J., Peng, W., Moller, A., Song, Y., Stockli, D.F., Stevens, T., Horton, B., Liu, S., Bird, A., Oalman, J., Gong, H., and Fang, X., 2014, Provenance of the Upper Miocene–Pliocene red clay deposits of the Chinese Loess Plateau: *Earth and Planetary Science Letters*, v. 407, p. 35–47, doi:10.1016/j.epsl.2014.09.026.
- Nie, J., Stevens, T., Rittner, M., Stockli, D., Garzanti, E., Limonta, M., et al., 2015, Loess plateau storage of northeastern Tibetan Plateau-derived Yellow River

- sediment: *Nature Communications*, v. 6, p. 8511, doi:10.1038/ncomms9511.
- Peizhen, Z., Molnar, P., and Downs, W.R., 2001, Increased sedimentation rates and grain sizes 2–4 Myr ago due to the influence of climate change on erosion rates: *Nature*, v. 410, p. 891–897, doi:10.1038/35073504.
- Porter, S., 2001, Chinese loess record of monsoon climate during the last glacial-interglacial cycle: *Earth-Science Reviews*, v. 54, p. 115–128, doi:10.1016/S0012-8252(01)00043-5.
- Porter, S., and An, Z., 1995, Correlation between climate events in the North Atlantic and China during the last glaciation: *Nature*, v. 375, p. 305–308, doi:10.1038/375305a0.
- Pullen, A., Kapp, P., McCallister, A., Chang, H., Gehrels, G., Garzzone, C., Heermance, R., and Ding, L., 2011, Qaidam Basin and northern Tibetan Plateau as dust sources for the Chinese Loess Plateau and paleoclimatic implications: *Geology*, v. 39, p. 1031–1034, doi:10.1130/G32296.1.
- Pullen, A., Ibanez-Mejia, M., Gehrels, G., Ibanez-Mejia, J., and Pecha, M., 2014, What happens when  $n = 1000$ ? Creating large- $n$  geochronological datasets with LA-ICP-MS for geologic investigations: *Journal of Analytical Atomic Spectrometry*, v. 29, p. 971–980, doi:10.1039/c4ja00024b.
- Pye, K., 1995, The nature, origin and accumulation of loess: *Quaternary Science Reviews*, v. 14, p. 653–667, doi:10.1016/0277-3791(95)00047-X.
- Qiang, X., An, Z., Song, Y., Chang, H., Sun, Y., Liu, W., Ao, H., Dong, J., Fu, C., Wu, F., Lu, F., Cai, Y., Zhou, W., Cao, J., Xu, X., and Ai, L., 2011, New eolian red clay sequence on the western Chinese Loess Plateau linked to onset of Asian desertification about 25 Ma ago: *Science China, Earth Science*, v. 54, p. 136–144.
- Roe, G., 2009, On the interpretation of Chinese loess as a paleoclimate indicator: *Quaternary Research*, v. 71, p. 150–161, doi:10.1016/j.yqres.2008.09.004.
- Rohrmann, A., Heermance, R., Kapp, P., and Cai, F., 2013, Wind as the primary driver of erosion in the Qaidam Basin, China: *Earth and Planetary Science Letters*, v. 374, p. 1–10, doi:10.1016/j.epsl.2013.03.011.
- Song, Y., Fang, X., King, J.W., Li, J., Naoto, I., and An, Z., 2014, Magnetic parameter variations in the Chaona loess/paleosol sequences in the central Chinese Loess Plateau, and their significance for the middle Pleistocene climate transition: *Quaternary Research*, v. 81, p. 433–444, doi:10.1016/j.yqres.2013.10.002.
- Stacey, J.S., and Kramers, J.D., 1975, Approximation of terrestrial lead isotope evolution by a two-stage model: *Earth and Planetary Science Letters*, v. 26, p. 207–221, doi:10.1016/0012-821X(75)90088-6.
- Stevens, T., and Lu, H., 2009, Optically stimulated luminescence dating as a tool for calculating sedimentation rates in Chinese loess: Comparisons with grain-size records: *Sedimentology*, v. 56, p. 911–934, doi:10.1111/j.1365-3091.2008.01004.x.
- Stevens, T., Palk, C., Carter, A., Lu, H., and Clift, P., 2010, Assessing the provenance of loess and desert sediments in northern China using U-Pb dating and morphology of detrital zircons: *Geological Society of America Bulletin*, v. 122, p. 1331–1344, doi:10.1130/B30102.1.
- Stevens, T., Carter, A., Watson, T., Vermeesch, P., Ando, S., Bird, A., Lu, H., Garzanti, E., Cottam, M., and Sevastjanova, I., 2013, Genetic linkage between the Yellow River, the Mu Us Desert and the Chinese Loess Plateau: *Quaternary Science Reviews*, v. 78, p. 355–368, doi:10.1016/j.quascirev.2012.11.032.
- Sun, D., Su, R., Bloemendal, J., and Lu, H., 2008, Grain-size and accumulation rate records from late Cenozoic aeolian sequences in northern China: Implications for variations in the East Asian winter monsoon and westerly atmospheric circulation: *Palaeogeography, Palaeoclimatology, Palaeoecology*, v. 264, p. 39–53, doi:10.1016/j.palaeo.2008.03.011.
- Sun, D., Zhang, Y., Han, F., Zhang, Y., Yi, Z., Li, Z., Wang, F., Wu, S., and Li, B., 2011, Magnetostratigraphy and palaeoenvironmental records for a late Cenozoic sedimentary sequence from Lanzhou, northeastern margin of the Tibetan Plateau: *Global and Planetary Change*, v. 76, p. 106–116, doi:10.1016/j.gloplacha.2010.12.006.
- Sun, J., 2002, Provenance of loess material and formation of loess deposits on the Chinese Loess Plateau: *Earth and Planetary Science Letters*, v. 203, p. 845–859, doi:10.1016/S0012-821X(02)00921-4.
- Sun, J., Zhang, M., and Liu, T., 2001, Spatial and temporal characteristics of dust storms in China and its surrounding regions, 1960–1999: Relations to source area and climate: *Journal of Geophysical Research*, v. 106, p. 10,325–10,333, doi:10.1029/2000JD900665.
- Sun, Y., Lu, H., and An, Z., 2006, Grain size of loess, palaeosol and red clay deposits on the Chinese Loess Plateau: Significance for understanding pedogenic alteration and palaeomonsoon evolution: *Palaeogeography, Palaeoclimatology, Palaeoecology*, v. 241, p. 129–138, doi:10.1016/j.palaeo.2006.06.018.
- Sweeney, M.R., and Mason, J.A., 2013, Mechanisms of dust emission from Pleistocene loess deposits, Nebraska, USA: *Journal of Geophysical Research—Earth Surface*, v. 118, p. 1460–1471.
- Toggweiler, J., and Russell, J., 2008, Ocean circulation in a warming climate: *Nature*, v. 451, p. 286–288, doi:10.1038/nature06590.
- Vandenbergh, J., 2013, Grain size of fine-grained wind-blown sediment: A powerful proxy for process identification: *Earth-Science Reviews*, v. 121, p. 18–30, doi:10.1016/j.earscirev.2013.03.001.
- Vandenbergh, J., Renssen, H., van Huissteden, K., Nugteren, G., Konert, M., Lu, H., Dodonov, A., and Buylaert, J.-P., 2006, Penetration of Atlantic westerly winds into Central and East Asia: *Quaternary Science Reviews*, v. 25, p. 2380–2389, doi:10.1016/j.quascirev.2006.02.017.
- Vermeesch, P., 2004, How many grains are needed for a provenance study?: *Earth and Planetary Science Letters*, v. 224, p. 441–451, doi:10.1016/j.epsl.2004.05.037.
- Vermeesch, P., 2012, On the visualisation of detrital age distributions: *Chemical Geology*, v. 312–313, p. 190–194, doi:10.1016/j.chemgeo.2012.04.021.
- Vermeesch, P., 2013, Multi-sample comparison of detrital age distributions: *Chemical Geology*, v. 341, p. 140–146, doi:10.1016/j.chemgeo.2013.01.010.
- Vermeesch, P., and Garzanti, E., 2015, Making geological sense of ‘Big Data’ in sedimentary provenance analysis: *Chemical Geology*, v. 409, p. 20–27, doi:10.1016/j.chemgeo.2015.05.004.
- van Loon, A., 2006, Lost loesses: *Earth-Science Reviews*, v. 74, p. 309–316, doi:10.1016/j.earscirev.2005.10.005.
- Wang, J., Wang, Y.J., Liu, Z.C., Li, J.Q., and Xi, P., 1999, Cenozoic environmental evolution of the Qaidam Basin and its implications for the uplift of the Tibetan Plateau and the drying of Central Asia: *Palaeogeography, Palaeoclimatology, Palaeoecology*, v. 152, p. 37–47, doi:10.1016/S0031-0182(99)00038-3.
- Wang, L., Lü, H.Y., Wu, N.Q., Li, J., Pei, Y.P., Tong, G.B., and Peng, S.Z., 2006, Palynological evidence for late Miocene–Pliocene vegetation evolution recorded in the red clay sequence of the central Chinese Loess Plateau and implication for palaeoenvironmental change: *Palaeogeography, Palaeoclimatology, Palaeoecology*, v. 241, p. 118–128, doi:10.1016/j.palaeo.2006.06.012.
- Wang, X., Dong, Z., Zhang, J., and Liu, L., 2004, Modern dust storms in China: An overview: *Journal of Arid Environments*, v. 58, p. 559–574, doi:10.1016/j.jaridenv.2003.11.009.
- Weislogel, A., Graham, S., Chang, E., Wooden, J., and Gehrels, G., 2010, Detrital zircon provenance from three turbidite depocenters of the Middle–Upper Triassic Songpan–Ganzi complex, central China: Record of collisional tectonics, erosional exhumation, and sediment production: *Geological Society of America Bulletin*, v. 122, p. 2041–2062, doi:10.1130/B26606.1.
- Wu, F., Fang, X., Ma, Y., Herrmann, M., Mosbrugger, V., An, Z., and Miao, Y., 2007, Plio–Quaternary stepwise drying of Asia: Evidence from a 3-Ma pollen record from the Chinese Loess Plateau: *Earth and Planetary Science Letters*, v. 257, p. 160–169, doi:10.1016/j.epsl.2007.02.029.
- Xiao, G., Zong, K., Li, G., Hu, Z., Dupont-Nivet, G., Peng, S., and Zhang, K., 2012, Spatial and glacial-interglacial variations in provenance of the Chinese Loess Plateau: *Geophysical Research Letters*, v. 39, p. L20715, doi:10.1029/2012GL053304.
- Yan, Y., Sun, Y., Chen, H., and Ma, L., 2014, Oxygen isotope signatures of quartz from major Asian dust sources: Implications for changes in the provenance of Chinese loess: *Geochimica et Cosmochimica Acta*, v. 139, p. 399–410, doi:10.1016/j.gca.2014.04.043.
- Yin, A., Dang, Y.-Q., Zhang, M., Chen, X.-H., and McRivette, M.W., 2008, Cenozoic tectonic evolution of the Qaidam Basin and its surrounding regions (Part 3): Structural geology, sedimentation, and regional tectonic reconstruction: *Geological Society of America Bulletin*, v. 120, p. 847–876, doi:10.1130/B26232.1.

SCIENCE EDITOR: AARON CAVOSIE  
ASSOCIATE EDITOR: AN YIN

MANUSCRIPT RECEIVED 30 JUNE 2015  
REVISED MANUSCRIPT RECEIVED 9 NOVEMBER 2015  
MANUSCRIPT ACCEPTED 15 DECEMBER 2015

Printed in the USA